II-F Controllable Magnetic Properties of Ultrathin Magnetic Films Using Surface Chemical Techniques

Noble properties of magnetic thin films such as perpendicular magnetic anisotropy (PMA) and giant magentoresistance (GMR) have extremely attracted scientific and technological interests. The origin of perpendicular magnetic anisotropy of ultrathin metal films is not fully understood and is an important subject in fundamental physics but is useful for high-density recording media. The GMR property is already utilized for read-heads of hard disk drives, although quantitative understanding of the GMR is still to be improved. We have been investigating drastic changes of magnetic properties of ultrathin metal films by using surface chemical modification such as atoms/molecules adsorption on the surface. Especially, the microscopic mechanism of spin reorientation transitions induced by gaseous adsorption on magnetic film surfaces have been investigated by means of the synchrotron radiation x-ray magnetic circular dichroism (XMCD), the visible-light magneto-optical Kerr effect (MOKE) and the magnetization induced second harmonic generation (MSHG) techniques. A goal of these works is spin engineering by which the magnetization of ultrathin metal films and nanowires can be controlled artificially.

II-F-1 MOKE and XMCD Study on K Adsorption on Fe Ultrathin Films on Cu(001)

NAKAGAWA, Takeshi; WATANABE, Hirokazu; YOKOYAMA, Toshihiko

It is interesting to investigate whether electron donation to magnetic metal films induces the enhancement or suppression of magnetization. Especially, Fe could be a candidate whose magnetization is enhanced by electron donation. In the present work, we have studied the effect of K adsorption on *fct* (face-centered-tetragonal) Fe and Co grown on Cu(001) by means of the polar MOKE and the XMCD methods.

Figure 1 shows the MOKE intensity from 3 ML Fe on Cu(001) as a function of K coverage, which was measured during K deposition. With the increase in the K coverage, the MOKE intensity increases and at 0.1 ML K deposition it is maximized. More deposition leads to the suppression. The K coverage of 0.1 ML roughly corresponds to the work function minimum. Although the MOKE intensity is usually proportional to the magnetization, it could not be the case if the electronic structure changes drastically. In order to confirm the enhanced magnetization and to obtain more direct information, we have performed XMCD measurements at BL4B of UVSOR-II. Figure 2(a) shows the Fe *L*-edge XMCD. A small increase in the XMCD signals is actually found at the K coverage of 0.1 ML. Table 1 summarizes the results of the quantitative analysis. In both the Fe and Co cases, the number of 3*d* holes, which was estimated from the intensity of the white lines, is gradually reduced with the K coverage, this exemplifying the electron donation from K. In the Co case, the spin magnetic moment decreases monotonically with the K coverage. This finding is reasonable since the majority 3*d* band of *fcc* Co is fully occupied and the donated electron is transferred to the minority 3*d* bands, leading to the reduction of the spin magnetic moment of Co. On the contrary, the spin magnetic moment of Fe is maximized at 0.1 ML K. This verifies that the Fe spin magnetic moment is enhanced by a small amount of K deposition.

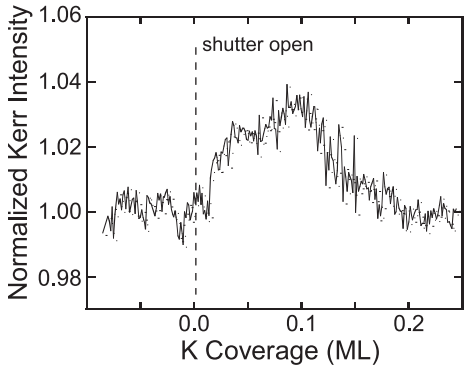

Figure 1. Polar MOKE intensity of 3 ML Fe/Cu(001) at 100 K as a function K deposition.

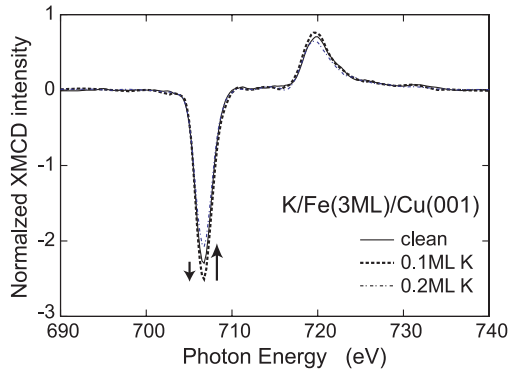

Figure 2. Fe *L*-edge XMCD of 3 ML Fe/Cu(001) (perpendicularly magnetized) at 100 K for the K coverages of 0.0, 0.1 and 0.2 ML.

Table 1. The results of the sum-rule analysis for 3 ML Fe and Co on Cu(001). 3*d* hole numbers and spin (m_s) and orbital (m_l) magnetic moments of Fe and Co are given.

	K dep. (ML)	$3d_{\mathrm{hole}}$ number	m_s (μ_B)	m_l (μ_B)
3 ML Fe	0.0	3.40	2.29	0.24
/Cu(001)	0.1	3.27	2.40	0.24
	0.2	3.00	1.91	0.17
3 ML Co	0.0	2.50	1.67	0.26
/Cu(001)	0.1	2.37	1.58	0.26
	0.2	2.27	1.50	0.29

II-F-2 Spin Reorientation Transition in Ag-Covered Co Films Grown on Vicinal Cu(001) Surface Studied by Means of XMCD

NAKAGAWA, Takeshi; WATANABE, Hirokazu; YOKOYAMA, Toshihiko

Magnetic thin films grown on vicinal surfaces exhibit strong uniaxial magnetic anisotropy; the magnetic property should be essentially different between the step-parallel and perpendicular directions. In this work, in order to obtain microscopic information on the spin reorientation transition in Ag-deposited Co films on Cu(1 1 17), we performed the longitudinal MOKE and XMCD experiments.

Figure 1 shows the magnetic hysteresis loops of MOKE. In the clean Co film, the magnetization curve along the //step direction exhibits normal rectangular shape, while that along the ⊥step direction shows a double loop with zero remanence, this implying the easy axis of the //step direction. On the contrary, the reverse is true for the 0.2 ML Ag-deposited Co film; the magnetic easy axis changes from //step to ⊥step, exhibiting clear spin reorientation transition. This results is identical with the previously reported work by Weber *et al.* [*Phys. Rev. B* **52**, R14400 (1995)].

Figure 2 shows the Co *L*-edge XMCD. The intensities of the L_{III}- and L_{II}-edge peaks exhibit clear difference between the clean and Ag-deposited Co films. Although the difference is rather small, one can find that larger orbital magnetic moments give the magnetic easy axis from the detailed sum-rule analysis: for clean Co, $m_l^{//} = 0.246\ \mu_B$ and $m_l^{\perp} = 0.225\ \mu_B$, while for Ag-deposited Co, $m_l^{//} = 0.200\ \mu_B$ and $m_l^{\perp} = 0.218\ \mu_B$. Moreover, we have determined the inclination angle of the easy axis. Figure 3 shows the results of the XMCD variation. The *x*-intercept corresponds to the easy axis, where 0° and –4.8° respectively mean parallel to the physical plane and to the terrance plane. The present finding in Figure 3 concludes that the Ag deposition induces also the out-of-plane rotation of the easy axis from the physical surface plane (0°) to the terrance plane (–4.8°).

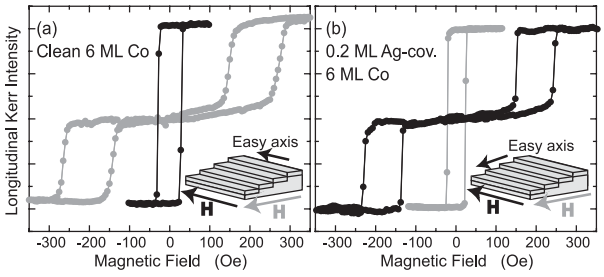

Figure 1. MOKE hysteresis loops of (a) clean and (b) Ag-deposited 6 ML Co/Cu(1 1 17) at 100 K.

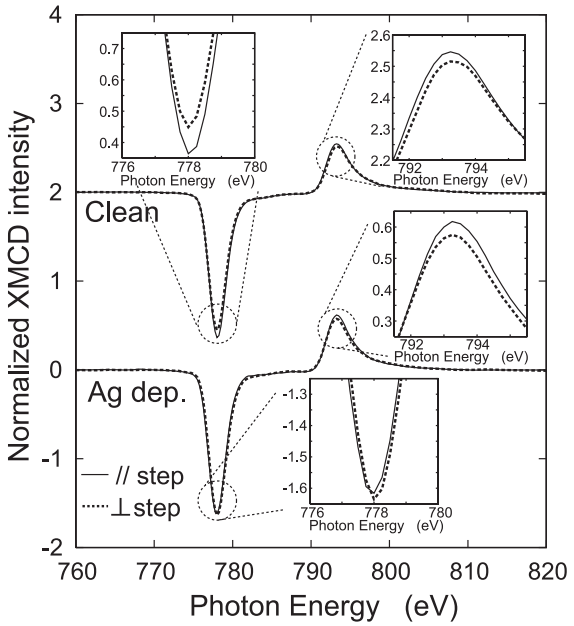

Figure 2. Co *L*-edge XMCD of 6 ML Co/Cu(1 1 17) at 100 K before and after 0.2 ML Ag deposition.

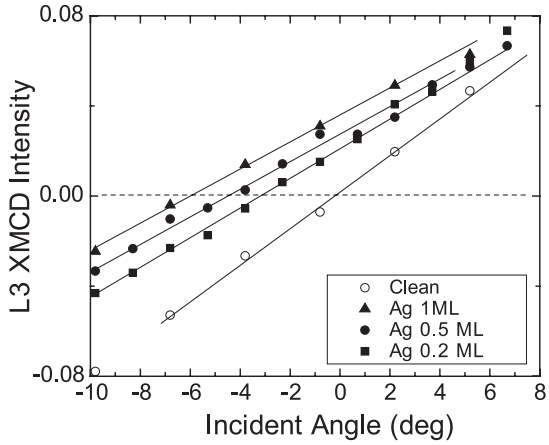

Figure 3. Angle dependence of Co L_{III}-edge XMCD intensity of 6 ML Co/Cu(1 1 17).

II-F-3 Drastic Magnetization Change Observed in NO Adsorption on Co/Cu(1 1 17)

NAKAGAWA, Takeshi; WATANABE, Hirokazu; YOKOYAMA, Toshihiko

Magnetic thin films grown on vicinal surfaces exhibit strong uniaxial magnetic anisotropy and the anisotropy could be modified by surface chemical treatments. In this work, we have investigated the effect of NO adsorption on uniaxial Co films grown on Cu(1 1 17) by means of the longitudinal MOKE and the XMCD experiments.

Figure 1 shows the magnetic hysteresis loops of longitudinal MOKE. In the clean Co film, the magnetization curve along the //step direction exhibits normal rectangular shape, while that along the ⊥step direction shows a double loop with zero remanence, this implying the presence of strong uniaxial magnetic anisotropy and the easy axis of the //step direction. However, drastic

changes can be seen after NO adsorption. The coercivity is reduced noticeably, and the //step and ⊥step loops are completely identical, this indicating the disappearance of the inherent uniaxial anisotropy and the appearance of almost fourfold symmetric magnetic anisotropy. Such a change is much more drastic than the film on flat Cu(001).

Figure 2 shows the Co *L*-edge XMCD. The intensities of the L_{III}- and L_{II}-edge peaks exhibit clear difference between the clean and NO-adsorbed Co films. From the detailed sum-rule analysis, one can find that in a clean Co film a larger orbital magnetic moments give the magnetic easy axis (for clean Co, $m_l^{//}$ = 0.256 μ_B and $m_l^{\perp}$ = 0.224 μ_B), while the orbital magnetic moments are essentially the same between the //step and ⊥step directions after NO adsorption ($m_l^{//}$ = 0.116 μ_B and $m_l^{\perp}$ = 0.123 μ_B). This is consistent with the longitudinal MOKE results.

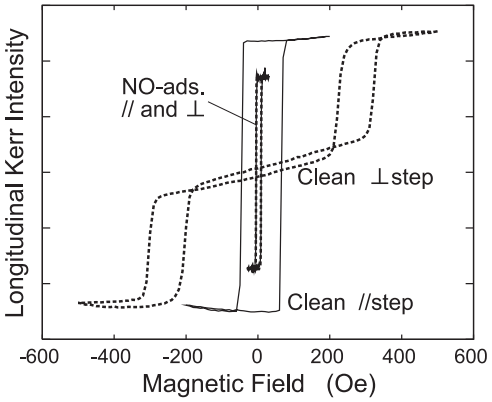

Figure 1. Longitudinal MOKE hysteresis loops of clean and NO-adsorbed 6 ML Co films on Cu(1 1 17) at 100 K.

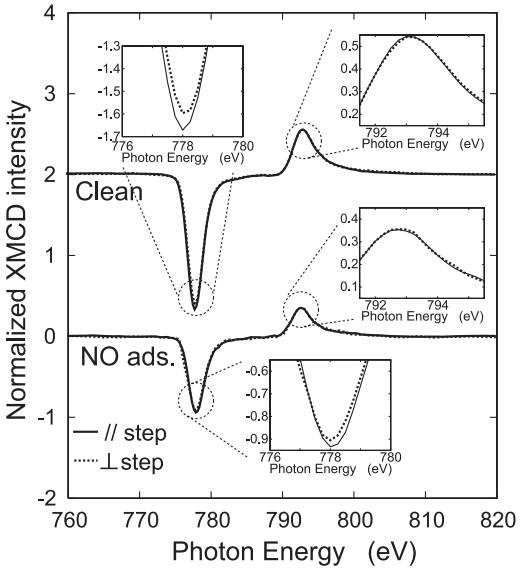

Figure 2. Co *L*-edge XMCD of 6 ML Co/Cu(1 1 17) at 100 K before and after 0.5 ML NO adsorption.

II-F-4 Direct Observation of Biquadratic Exchange Interaction in Fe/Ni/Cu(001) by Using MSHG

NAKAGAWA, Takeshi; YOKOYAMA, Toshihiko

Ultrathin *fcc* Fe films are known to exhibit various peculiar magnetic properties since *fcc* Fe shows ferromagnetism and antiferromagnetism depending on very small changes in the lattice constant. Very recently, Liu *et al*. [*Phys. Rev. B* **65** 224413 (2002)] observed an exchange bias in Fe/Ni/Cu(001) from their MOKE measurements and proposed that in there should exist biquadratic exchange interaction (perpendicular spin-spin interaction is stable). This observation is quite interesting since in the Fe/Ni system all the magnetic metal atoms are directly bonded with each other and Heisenberg exchange interaction is usually expected. In this work, we have obtained direct proof for the perpendicular magnetization in this system by using the MSHG technique exploited in this group.

Figure 1 shows the longitudinal MOKE and MSHG results. The curves of MOKE and MSHG Pin-Sout (S-polarization incidence and P-polarization reflection) give the magnetization along the magnetic field, while those of Pin-Pout and Sin-Pout the magnetization perpendicular to the magnetic field within the film plane. Actually, the perpendicular components are observed especially for 3.3 ML Fe. Figure 2 shows the remanent magnetization and the coercive field as a function of Fe coverage. Two minima at ~4 and ~8 ML Fe can be seen. We can recognize that each Fe layer interacts with the adjacent layer so that the magnetization directions are perpendicular with each other; 4 and 8 ML Fe films correspond to one and two periodic antiferromagnets, respectively. The presence of the biquadratic exchange interaction in this system is experimentally proved.

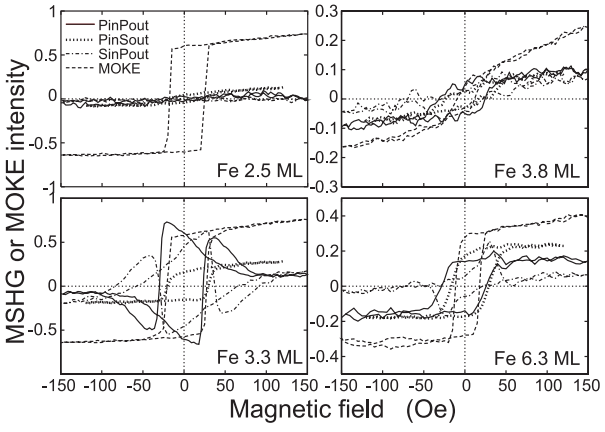

Figure 1. Magnetization curves given by the longitudinal MOKE and the MSHG (Pin-Pout, Sin-Pout and Pin-Sout) for Fe/Ni(7 ML)/Cu(001).

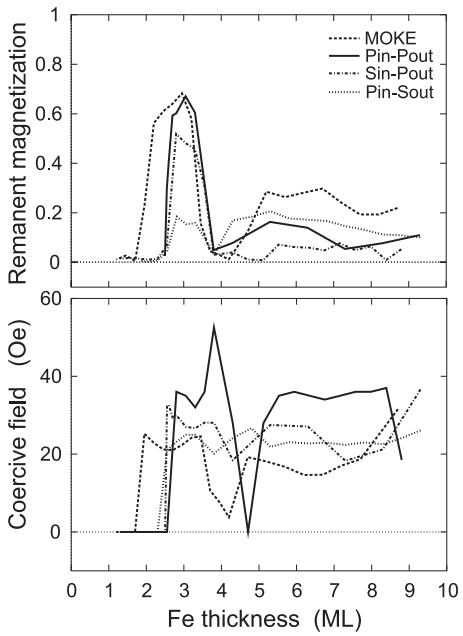

Figure 2. Remanent magnetization and the coercive field as a function of Fe coverage given by the longitudinal MOKE and the MSHG.

II-G Local Structures of Molecular-Based Magnetic Materials Studied by X-Ray Absorption Fine Structure Spectroscopy

Molecular-based magnets provide noble properties such as quantum tunneling of magnetization, photoinduced magnetism *etc*. In order to understand fully the magnetic properties, structural information is indispensable. Although usually the X-ray diffraction analysis of single crystals is the most appropriate to determine the three-dimensional structure, there exist several cases when the X-ray diffraction analysis cannot be applied: the crystal structure is disordered, single crystals are hardly obtainable, and so forth. We have been studying local structures and electronic properties of interesting molecular magnets by means of X-ray absorption fine structure (XAFS) spectroscopy.

II-G-1 Molecular Structure of Single-Molecule Magnet $Mn_{11}Cr$, $Mn_{11}Cr^{-}$ and $Mn_{10}Fe_2$

YOKOYAMA, Toshihiko; HACHISUKA, Hidekazu[1]; AWAGA, Kunio[1]
([1]Nagoya Univ.)

[*Phys. Rev. B* **70**, 104427 (2004)]

Single-molecular magnet of $[Mn_{12}(AcO)_{16}(H_2O)_4]$ (Ac = CH_3COO) has extensively been investigated because of its interesting properties such as stepwise magnetization due to the quantum tunneling effect. One of the outstanding features of molecular magnets is the ease of chemical modification. Recently, molecular magnets of $Mn_{11}Cr$ ($[Mn_{11}CrO_{12}(AcO)_{16}(H_2O)_4]$) $Mn_{10}Fe_2$ ($[Mn_{10}Fe_2O_{12}(AcO)_{16}(H_2O)_4]$) and $Mn_{11}Cr^{-}$ ($[(Ph)_4P][Mn_{11}CrO_{12}(PhCOO)_{16}(H_2O)_4]$) were synthesized. Although the single crystal x-ray diffraction analyses have been performed, the location of Cr or Fe cannot be determined because of the crystalline disorder of their positions. In such a case, EXAFS is the most suitable technique to determine the molecular structure.

Figure 1 depicts the Fourier transforms of the EXAFS functions of $Mn_{11}Cr$. The x-ray molecular structure gives the average structure where Cr is not distinguished from Mn. There exist three types of Cr/Mn sites: Sites **1**, **2**, and **3**, as shown in Figure 2. Site **1** is occupied by Mn^{4+} ions, while Sites **2** and **3** are by Mn^{3+}. The Fourier transform of Cr is similar to the simulated one of Site **3**. It is thus concluded that, in $Mn_{11}Cr$, Cr^{3+} exclusively occupies Site **3**, the tilted site for Mn^{3+} in the Mn_{12} skeleton. The magnitude of the experimental Cr–O peak is much stronger than that of the theoretical one of Site **3**, because the Mn^{3+} ion in Site **3** exhibits significantly distorted octahedron due to the Jahn-Teller effect, resulting in the suppression of the Mn–O contribution in the simulation. On the contrary, the Cr^{3+} ion shows no Jahn-Teller distortion, yielding more intense Cr–O contribution in the Fourier transform.

Essentially the same results are obtained for $Mn_{10}Fe_2$ and $Mn_{11}Cr^{-}$, and in conclusion, the Cr/Fe ion locates exclusively at Site **3** with normal valency of Cr/Fe(III).

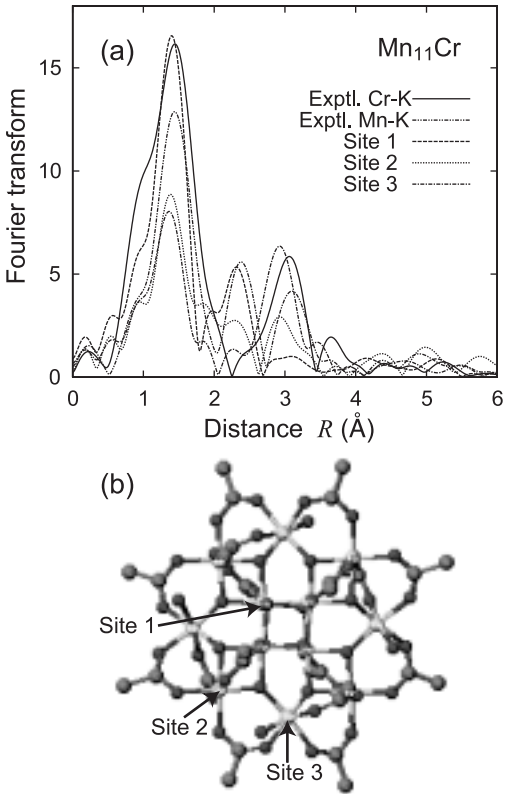

Figure 1. (a) Fourier transforms of the Cr (solid line) and Mn (dot-dot-dashed) K-edge EXAFS functions, together with the theoretical simulation results for Sites **1** (dotted), **2** (dot-dashed) and **3** (dashed). (b) Molecular structure of Mn_{12}. Mn atoms locate three inequivalent Sites **1**, **2** and **3**.

II-G-2 Photoinduced Phase Transition of CuMo Cyanides Studied by XAFS Spectroscopy

MA, Xiao-Dong; YOKOYAMA, Toshihiko; HOZUMI, Toshiya[1]; HASHIMOTO, Kazuhito[1]; OHKOSHI, Shin-ichi[1]
([1]Univ. Tokyo)

[*Phys. Rev. B* **72**, 094107 (2005)]

Prussian-blue analogues often exhibit noble magnetic properties such as photoinduced magnetization. In this work, we have investigated the local structures and the electronic states mainly of the photoinduced phases of two CuMo cyanides of $Cu_2Mo(CN)_8 \cdot 8H_2O$ (**1**) and $Cs_{0.5}Cu_{1.75}Mo(CN)_8 \cdot 1.5H_2O$ (**2**) by means of XAFS. Usually, the photoinduced phase at low temperature is considered to be structurally identical to that of the corresponding high-temperature phase. However the photoinduced phase is an essentially new state for these two CuMo compounds because in the low-temperature phase even at room temperature they are likely to decompose with the temperature rise before thermally driven phase transition takes place.

Figure 1(a) shows the Cu *K*-edge spectra of samples (**1**) and (**2**) before and after photoirradiation, together with the reference spectra of $Cu^{(I)}{}_2O$ and $Cu^{(II)}O$. One can immediately conclude that the Cu atoms in samples (**1**) and (**2**) are divalent before photoirradiation, and monovalent Cu appears after photoirradiation. Figure 1(b) shows the Mo and Cu *K*-edge EXAFS Fourier transforms of sample (**2**). Overall, one can find that the features of the initial low-temperature and photoinduced phases are almost identical. The interatomic distances are almost the same between the initial and the photoinduced phases. Differences between the low-temperature and the photoinduced phases can however be detected in the amplitude in the EXAFS oscillation. The coordination numbers of the Mo–N, Mo–Cu, and Cu–Mo shells are found reduced, while those of the Mo–C, Cu–N, and Cu–C shells as well as the first-nearest neighbor Mo–C and Cu–N shells are kept constant. The latter implies enhancement of the static Debye-Waller factors. The reduction of the coordination numbers for the Mo–N, Mo–Cu, and Cu–Mo shells may be ascribed not to the bond breaking but to the bond bending. One can qualitatively conclude that due to the photoirradiation the Mo–CN bond is bent, while the Cu–NC bond angle is kept unchanged.

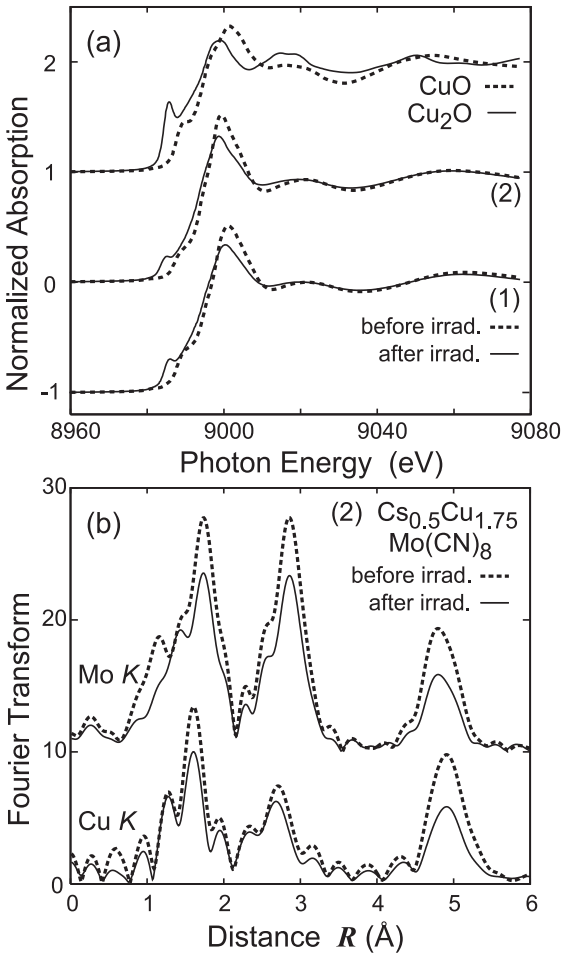

Figure 1. (a) Cu *K*-edge X-ray absorption spectra of samples (**1**) and (**2**), together with those of Cu_2O and CuO. (b) Fourier transforms of the Mo and Cu *K*-edge EXAFS oscillation functions of sample (**2**) at 30 K before and after photoirradiation.